Sl. No.	IIT Ropar List of Recent Publications with Abstract
110.	Coverage: September, 2025
A	Book Chapter(s)
	Crop health monitoring and yield estimation through geospatial technology R Singh, V Gautam, S Pathak - Geo-Data Revolution: Advances in Spatial Analysis and Natural Hazard Mapping: Book Chapter, 2025
1.	Abstract: Crop yield model has been a big leap in remote sensing and understanding the crop health. By understanding the crop health, we can relate yield accordingly. Different crop yielding models have been built to justify their results; all of the models go through a rigid process of testing. The yield of every model is not a proper result but an estimate, which is accurate enough to plan further. The majority of the models rely on NDVI or a vegetation index to work with. In this chapter, we are going to work with a crop model to calculate the yield of the state of Indiana. The yield is to be calculated of corn and soybeans of the year 2023. The model used in the chapter was a predefined model that was used for the state of Illinois, and now further we will check its accuracy on the state of Indiana. The output of the model was 224 bushels minimum, whereas the average was 204 bushels for the corn for the year 2023 (August). The output for the corn was highest with 56 bushels per acre, while the initial yield was 61 bushels per acre. The model does give us an insight into the yield that is to be procured. But we should generally consider it as an estimate but not the initial result of the harvest.
2.	Crop yield estimation in Indiana using a semi-physical model K Sen, V Gautam, S Pathak - Geo-Data Revolution: Advances in Spatial Analysis and Natural Hazard Mapping: Book Chapter, 2025 Abstract: For planning and food safety, farmers and economists depend on precise crop production projections. Models based on remote sensing have proven to be successful in predicting yields on a wide scale, but there is still a significant obstacle to their transferability across diverse geographic areas. In this work, we used 5 years of data (2019–2023) to predict corn and soybean yields in Indiana, USA, using a semi-physical modelling approach. The method described here utilizes photosynthetically active radiation (PAR), light use efficiency (LUE), and fraction of absorbed photosynthetically active radiation (FPAR) in calculating net primary productivity (NPP). Water stress, temperature stress, vegetative growth factor, and maximum light efficiency are used to compute the LUE. For corn and soybean, the model's coefficient of determination (R²) was 0.76 and 0.56, respectively, with root mean square errors (RMSE) of 0.82 and 1.42 tons/ha. The results show the remote sensing model provided the yield for a region and made the model for enhancing the agricultural decision-making and resource management. The further improvement of this model parameter and high-resolution data can make the model more predictable for a
3.	regional yield, and we can use it for real-time crop monitoring. Ecosystem services and sustainable development goals: A comprehensive review NG Paswan, S Pathak - Geo-Data Revolution: Advances in Spatial Analysis and Natural Hazard Mapping: Book Chapter, 2025
	Abstract: Ecosystem services (ES) are important for human life survival. A complete knowledge of ES is required for achieving the Sustainable Development Goals. Initially, the study examines the importance of ES for human well-being and sustainable development, highlighting global degradation of these services. Land use changes, urbanization, and climate change are all important key elements that disturb biological and chemical processes in the ecosystem. Further, the study underscores the role of Remote Sensing (RS) and Geographic Information Systems (GIS) in ecosystem mapping and monitoring. Integrating remote sensing data with field and socioeconomic information offers a comprehensive approach for ecosystem service evaluation, shaping research and policy directions for sustainable resource management and conservation. Additionally, the

study delved into the intricate connections between different ecosystem services, underscoring the necessity for integrative, scalable methods to manage and safeguard ecosystems. The study also addresses the challenges posed by global degradation of these services and advocates for scalable techniques to ensure their preservation, thereby promoting sustainable development on a global scale. The review highlights that integrative and scalable management approaches are essential to safeguard these services against ongoing global degradation. By fostering a deeper understanding of the intricate linkages between ecosystem services and sustainable development, this comprehensive review calls for concerted efforts from policymakers, scientists, and communities to implement effective strategies that ensure both ecological and human well-being for future generations.

Estimation of surface runoff of Satluj sub-basin of Bilaspur and parts of Mandi, Shimla, Solan, Himachal Pradesh, India

S Bauddh, R Mahto, **NG Paswan** - Geo-Data Revolution: Advances in Spatial Analysis and Natural Hazard Mapping: Book Chapter, 2025

Abstract: The runoff estimation is essential for managing water resources, assessing flood risks, and planning environmental strategies. This chapter explores a comprehensive methodology to estimate surface runoff in Satluj River Basin in parts of Bilaspur District of Himachal Pradesh. The total area of study is approx. 1098.77 km². The RS and GIS technologies were used for calculating surface runoff. The rainfall data (daily and monthly) of required area (from June 2023 to September 2023) was collected from India-WRIS website and used to predict the runoff using the soil conservation service-curve number (SCS-CN) method, advanced by the USDA Natural Resources Conservation Service (NRCS). The curve number (CN) is calculated using Antecedent Moisture Condition II (AMC-II) by integrating hydrologic soil groups (HSGs) and LULC categories. For that, satellite imagery, digital elevation models (DEMs), hydrological soil data, and precipitation data are merged with geospatial technologies. These tools are used to classify LULC, extract drainage networks, delineate basins, and estimate surface runoff in the area of interest. The surface runoff map has been generated with low and high of 865.75 mm and 1344.86 mm, respectively, for the monsoon season in the area of interest. This information can be used to develop required water and soil conservation plans.

4.

5.

Evolution of morphometric features and river course of Ganges Basin: A case study in the Upper Ganga Basin

V Narwal, **S Pathak** - Geo-Data Revolution: Advances in Spatial Analysis and Natural Hazard Mapping: Book Chapter, 2025

Abstract: The study investigates the changes in the physical characteristics and pathway of the Ganges River in its upper basin. It aims to explore the geomorphological development of the Upper Ganga River area between Rudraprayag and Rishikesh, using data from 2012 and 2024, with 2012 serving as the baseline year. The study highlights lateral shifts in the riverbanks caused by human activities and natural disasters. The shifts observed in 2014 demonstrate the impact of the 2013 disaster in the Mandakini River, offering insight into the immediate effects on the riverbanks. The 2024 data provides a current perspective, aiding in the understanding of long-term changes over time. This research focuses on identifying alterations in the river's course and morphometric features over time, analyzing data from specific periods to understand the impacts of events such as natural disasters and infrastructural developments. By comparing historical and recent data, the study aims to provide insights into the dynamic nature of the river system and the factors driving its evolution.

Flood risk assessment and hydrological response modelling in the Bhimgoda Region, Upper Ganga Basin, India

6. **Kajal, S Pathak** - Geo-Data Revolution: Advances in Spatial Analysis and Hazard Mapping: Book Chapter, 2025

Abstract: Flooding is one of the most devastating natural disasters, significantly impacting human lives, infrastructure, and ecosystems. This study focuses on the Upper Ganga Basin, a region highly vulnerable to flooding. The research employs hydrological and hydraulic modelling using HEC-HMS and HEC-RAS to simulate flood events and map inundation patterns for a region of the Upper Ganga Basin whose outlet point was taken at the Bhimgoda barrage. Daily precipitation data acquired from IMD from 2006 to 2023 were used as an input for HEC-HMS and in the construction of IDF curves. This study was conducted for a return period of 2, 5, 10, 25, 50, and 100 years. Peak discharge for different return periods was acquired from HEC-HMS, which was demonstrated as a hydrograph. This peak discharge value was used as an input in HEC-RAS, which in turn was used to formulate flood inundation maps for different return periods. This study investigates the geomorphological changes induced by extreme floods and evaluates their impact on the nearby region. Flood inundation maps derived from the model can be utilized to assess the spatial extent of flooding under various scenarios, providing critical insights into high-risk zones. These findings can further be utilized to make informed flood management strategies and enhance early warning systems in flood-prone areas.

Implementing and validating a remote sensing-driven crop yield estimation model in Illinois, USA V Gautam, S Giri, S Pathak - Geo-Data Revolution: Advances in Spatial Analysis and Natural Hazard Mapping: Book Chapter, 2025

Abstract: Accurate and timely estimation of crop yields is crucial for agricultural planning, food security, and economic forecasting. Remote sensing-based models have proven effective tools for large-scale crop yield prediction. This study investigates the transferability and robustness of a remote sensing-driven crop yield estimation model across diverse geographical regions within the U.S. Midwest. Originally developed for Iowa, the crop yield estimation model was adapted for use in Illinois while retaining its original structure and coefficients. The model integrates time-series Normalized Difference Vegetation Index (NDVI) data from Landsat 8–9, with surface parameters including land surface temperature, soil moisture, and precipitation. The study focused on corn and soybeans, the predominant crops in the region. The adapted model projected average yields of 280 bushels per acre for corn and 50 bushels per acre for soybeans across Illinois. These projections align closely with historical yield data and fall within the expected ranges for the state. Spatial analysis identified yield patterns that align with known variations in agricultural productivity variations across Illinois, particularly showing higher yields in the fertile central areas. Our findings have significant implications for large-scale crop yield forecasting and agricultural decision-making. The model's demonstrated transferability provides a cost-effective method for estimating yields across vast geographical areas, eliminating the necessity for extensive local calibration.

7.

8.

Modelling of urban ecosystem services in Chandigarh using InVEST modelling
S Rohilla, NG Paswan, S Pathak - Geo-Data Revolution: Advances in Spatial Analysis and
Natural Hazard Mapping: Book Chapter, 2025

Abstract: Ecological development of an area is impacted considerably by urban growth, which leads to climate change. Climate change is a major issue in the twenty-first century, and by absorbing CO₂ from the atmosphere through photosynthesis, urban green space can be a major solution to climate change. We selected the Union Territory of Chandigarh for ecosystem service study, which has a population of more than 1.2 million. Management of carbon in green space is the best strategy for climate change mitigation and microclimate regulation within the city. This study aims to quantify carbon storage and sequestration in both physical and economic contexts. The InVEST model was used for carbon sequestration from 2013 to 2023. InVEST utilized the LUILC map and the carbon pool value and aggregated them. Remote sensing, along with the GIS tool, were used for the preparation of data input—remote sensing for land use and land cover of the study area, and GIS for the visualization of the investment output. The amount of green space was found to have decreased by 13% from the base year, and the amount of built-up areas increased approximately 21% at the expense of green cover. The results of the InVEST model show a

	decrease in carbon storage in this time period from 5.8×10^5 Mg in 2013 to 4.9×10^5 Mg in 2023. Total carbon sequestration in Chandigarh is -8.2×10^4 Mg, indicating greater carbon emission than sequestration. Chandigarh experienced a marked decrease in green cover and agricultural land during this time period. The built-up area in Chandigarh increased by 21% from 2013 to 2023. The total net present value from 2013 to 2023 was -11.48 million dollars, showing a loss due to increased carbon emissions and reduced carbon sequestration, rendering ecological projects economically unviable. Analysis of the study shows the need for improved green cover management of the study area and advocates for a more sustainable way aproach to addressing climate change.
В	Conference Proceeding(s)
	A multilevel power converter for switched reluctance motors with integrated battery charging capability G Kumawat, S Payami - IEEE Energy Conversion congress & Exposition Asia (ECCE-Asia), 2025
9.	Abstract: This paper presents an integrated multilevel power converter (IMLPC) that includes battery charging functionality within a switched reluctance motor (SRM) drive system. By integrating the battery charger into the IMLPC design, the need for separate charging modules is eliminated. In motor operation, the IMLPC enhances energization and de-energization voltages, optimizing SRM performance. During charging, it operates as an onboard charger (OBC), delivering power to the battery storage system directly from a standard AC source. The OBC functionality is achieved by reconfiguring the IMLPC into an interleaved bridgeless boost power factor correction circuit (IBBPFCC). The inductors required for the IBB-PFCC are created by reusing the SRM windings. Additionally, reconfigured winding currents result in zero net torque, ensuring that the rotor remains stationary during charging without the need for external braking. The simulation and experimental outcomes validate the efficacy of the proposed IMLPC for level-1 charging applications.
	A new strategy to detect and localize interturn short-circuit fault in medium-frequency-transformer of dual-active-bridge converter TJ Nistane, S Payami, K Jayaraman - IEEE Energy Conversion Congress & Exposition Asia (ECCE-Asia), 2025
10.	Abstract: The windings of medium-frequency transformer (MFT) in the dual-Active-Bridge (DAB) converter are at huge risk of interturn (ITT) short-circuit fault due to rapid switching of high excitation voltages. Thus, it is crucial to quickly detect the online failure of winding at incipient level avoiding catastrophic conditions. Thus, the proposed work analyses DC link current of DAB converter under ITT fault and proposes a new online detection and localization strategy based on its variation for 4% of ITT fault. In the proposed work, the average and RMS of fault indicator obtained from difference of secondary and primary side DC link current are employed to detect and localize the ITT fault in MFT of the DAB converter. The presented work is supported via ANSYS simulation and validated for the hardware prototype of the DAB converter. Index Terms-Medium-frequency transformer (MFT), interturn (ITT) short-circuit fault, DAB converter, DC link current.
	BiQuad MIMO antenna system for UAV mobile base station in n28 5G NR band S Bansal, S Kumar, A Sharma - Third International Conference on Microwave, Antenna and Communication (MAC)
11.	Abstract: A two-element BiQuad MIMO antenna system working in the n28 5G NR band is presented as a mobile base station mounted on UAV. The proposed antenna system can provide an optimized solution for rapid deployment in disaster-affected areas to provide a temporary communication network for rescue operations. The two BiQuad antenna elements are oriented

towards $\pm 45^{\circ}$ with respect to the broad sight direction to enhance the communication coverage region.

<u>Dual-level adaptive sampling for enhanced few-shot medical image classification</u> **RR Chowdhury, U Niyaz, DR Bathula**... - IEEE 7th Symposium on Computers & Informatics (ISCI), 2025

Abstract: Medical image classification is often hindered by limited labeled data, making few-shot learning (FSL) a crucial approach. However, conventional FSL methods struggle with the high variance present in medical images. Consequently, we propose Dual-Level Adaptive Sampling (DLAS) to enhance FSL by strategically selecting the most informative class combinations and instances within each class. During training, our class sampling policy prioritizes challenging, underconfident classes to foster continual learning. Subsequently, instances within each class are weighted according to their true class probability, ensuring the selection of hard-to-classify samples for improved generalization. This dual-level strategy is seamlessly integrated into prototypical networks within a metric-based meta-learning framework and can be adapted to various few-shot learning models. We validate our approach through extensive quantitative and qualitative analyses on three benchmark medical imaging datasets-Derm7pt, PathMNIST, and ChestMNIST. Results show that our sampling framework significantly improves model generalization and classification performance compared to existing State-of-the-art methods.

Enhancing maritime multi object tracking with meta-data assisted re-identification

M Sharma, V Nageli, P Goyal... - International Conference on Computer Vision and Image Processing (CVIP 2024), 2025

Abstract: Detection, tracking, and re-identification (ReID) of objects in maritime environments in UAVs video stream presents significant challenges, particularly in search and rescue operations. In UAV based multi object tracking the ReID is hindered by the small object characteristics, sudden movements of the UAV's gimbal and limited appearance diversity. To address this, we proposed a integrated method which includes detection and tracking of maritime object classes: boats, swimmers, and floaters—using the challenging SeaDronesSee dataset. Our approach leverages spatio-temporal features by re-engineering the YOLOv7 network with Video Swin Transformer model to capture 1) object-related spatial features and 2) to enhances detection by learning spatio-temporal dependencies. Central to our method is the Metadata-Assisted Re-ID (MARe-ID) for object tracking, which harnesses critical metadata from UAV, like GPS, UAV altitude, and camera orientations etc. to enhance tracking accuracy. Our experiments demonstrate the state-of-the-art performance of our method in maritime object detection, tracking and Re-ID, with significant improvements observed on the SeaDronesSee dataset.

Focus shaping via flat optics

12.

13.

14.

R Menon, T Hayward, A Majumder...V Pal... - Proceedings Volume PC13595, Novel Optical Systems, Methods and Applications XXVIII, 2025

Abstract: Complex three-dimensional (3D) focus shaping plays a critical role in applications ranging from laser-based manufacturing to super-resolution optical microscopy. Traditional methods typically rely on multiple components (e.g., phase plates and objective lenses), which can be bulky and complex. In this work, we leverage inverse design to develop a single, patterned "flat optic" capable of producing precise 3D focus profiles. We demonstrate extended depth-of-focus spots with both Gaussian and square top-hat beam shapes, along with 3D hollow beams and other custom designs. These flat optics enable efficient laser marking, glass scribing, and laser cutting, and they function across all power levels and pulse widths—from continuous-wave (CW) to femtosecond—highlighting their versatility for a broad range of laser-based processes.

Harnessing large language models for sustainable materials and manufacturing: Frameworks, applications & innovations

A Pratap, N Sharma, N Sardana... - 2025 Seventh International Symposium on Computer, Consumer and Control (IS3C), 2025

Abstract: The integration of Large Language Models (LLMs) into materials and manufacturing offers a transformative approach to achieving ISO 9001 -compliant product quality, aligning with the goals of Industry 5.0. This work proposes MatManQ (Large Language Model in Material and Manufacturing for Product Quality and Control), a framework that leverages LLMs for quality control, assurance, and agentic Aldriven decision-making. A case study on alloy behavior using a self-curated dataset demonstrates the framework's capabilities. Five open-source LLMs-Mixtral-8x7B-327, TinyLlama-1.1B, deepset/roberta, Gemini, and FLAN-T5-were fine-tuned using a Retrieval-Augmented Generation (RAG) approach. Mixtral-8x7B-327 achieved the highest F1 score of 92.1%, attributed to its sparse Mixture-of-Experts architecture, enabling precise and efficient reasoning. The study highlights the potential of LLMs to unify material and manufacturing insights for enhanced product quality, while outlining key challenges and future directions for industrial deployment.

<u>Influence of grain size on formability in micro-incremental sheet forming of ultra-thin titanium grade 2 foils</u>

M Pal, A Agrawal, CK Nirala - All India Manufacturing Technology, Design and Research Conference (AIMTDR-2023), 2025

Abstract: Micro-incremental sheet forming (μISF) is a flexible manufacturing process and has advantages over existing micro-forming processes, due to its die-less nature of material deformation. In μISF, an ultra-thin foil is plastically deformed into a complex 3D geometry. It is precisely governed by the pre-defined toolpath of the forming tool on the surface of the foil. Due to size-effect, achieving high formability of the foils in micro-forming is difficult. This work investigates the deformation behavior of 100 μm thick CP-Ti Gr2 foils. The received foil is heat-treated at two different temperatures to obtain the foils with altered grain sizes. It was witnessed that the changes in annealing temperature and grain size enhanced the formability of the micro-parts. The foil with a higher grain size helped in increasing the fracture limit of the formed components.

Low profile planar multi-sector antenna array for drone swarm application

S Gupta, S Kumar, A Sharma - 2025 Third International Conference on Microwave, Antenna and Communication (MAC), 2025

Abstract: This paper presents a compact planar switched-beam multi-sector antenna array optimized for drone swarm applications, operating within the 2.1 GHz-2.6 GHz frequency range.

The proposed antenna array ensures complete azimuthal plane coverage through a directional radiation pattern while maintaining a compact form factor. Additionally, the isolation between adjacent antenna elements exceeds 15 dB in the operating band, minimizing mutual coupling effects. The design is validated through both simulations and experimental measurements, demonstrating excellent impedance matching and radiation performance. The proposed antenna is a promising solution for drone-based communication systems, offering efficient radiation characteristics with minimal structural impact.

<u>Using incremental LLM context for cost reduction in LLM-driven IoT applications</u> **A Sofat, B Sodhi** - European Conference on Software Architecture (ECSA 2025), 2025

Abstract: The LLM driven IoT applications need to handle time-sensitive information and dynamically evolving data. For example, the sensors in IoT systems send real-time data that must be taken into consideration by the LLM-driven application. The traditional architectures store such real-time IoT data in a database and re-prompt the LLM by suitably incorporating the new information on each request (or at designated time). Such an approach becomes inefficient

only some fraction of updates are relevant to the user's current question or context. (3) The application must preserve the conversation flow in a manageable size while still allowing new data to "flow in." In this paper we present an architecture that addresses these challenges by maintaining a lightweight "timeline" of recent and relevant "events". This design ensures that the LLM always sees a relevant snapshot of the most critical information at each step, without needing to ingest the entire stream of events every time. An important element in our architecture is the "event relevance scoring" module which allowed us to maintain a "sliding window" of the most crucial recent incoming sensors data. Our experiments show that, compared to the baseline, the proposed approach's response time is 15.41% faster and it generates 65.16% fewer tokens, which reduces token-based costs significantly. On average, it uses 5.41% less GPU and consumes 5.13% less CPU.

C Article(s)

A monitoring network for mitigating Himalayan glacial lake outburst floods
G Zhang... **RK Tiwari**... - Bulletin of the American Meteorological Society, 2025

Abstract: Glacial lake monitoring is urgently needed across the Himalaya due to the threat of glacial lake outburst floods (GLOFs). Furthermore, both the population and the infrastructure exposed to or dependent on these glacial lakes are increasing. However, there are a substantial number of glacial lakes in the Himalaya with potential transboundary GLOF impacts, and their remote high-altitude locations make monitoring extremely challenging, so existing field measurements are limited. Here, we propose a benchmark Himalayan glacial lake monitoring network 'HiGLMN' that will characterize glacial lakes by combining geomorphological signatures of GLOFs, monitoring triggers and mechanisms of dam failure and downstream impacts using insitu observations, remote sensing, and hydrodynamic modelling, and feed into early warning for disaster mitigation. We also provide existing practices to support the effectiveness and necessity and propose strategies for future data management. The monitoring network will contribute to robust GLOF risk management, early warning and mitigation.

A novel data generation scheme for surrogate modelling with deep operator networks

S Choubey, S Rahi, B Pal, M Agrawal - Engineering Applications of Artificial Intelligence, 2025

Abstract: Operator-based neural network architectures such as deep operator networks have emerged as a promising tool for the surrogate modelling of physical systems. In general, the training data for operator surrogate modelling are generated by solving partial differential equations using the finite element method. The computationally intensive nature of data generation is one of the major bottlenecks in deploying these surrogate models, hindering the deployment of these surrogate models in practical applications. In this study, we propose a novel methodology to alleviate the computational burden associated with training data generation for deep operator networks. Unlike the existing literature, the proposed framework for data generation does not use any partial differential equation integration strategy, such as the finite element method. In the proposed strategy, the primary field consistent with the boundary conditions is first generated randomly using Gaussian process regression. Thereafter, from the primary field, the input source field is calculated using second-order accurate finite difference techniques. The computation of the derivatives from the finite difference scheme is significantly less computationally intensive and easier to implement compared to integrating the underlying governing equations, thereby reducing the computational cost associated with generating training datasets. To validate the proposed approach, we employ heat equations as a model problem and develop the surrogate model for numerous boundary value problems.

AI-enhanced FES for foot drop: A novel biphasic charge-balanced stimulation approach

B Basumatary, RS Halder, AN Mallick, A Khokhar...R Kumar, AK Sahani - IEEE Access,
2025

20.

21.

Abstract: Foot drop is a neuromuscular condition that impairs a patient's ability to lift their foot while walking, leading to gait abnormalities and increased fall risk. Functional Electrical Stimulation (FES) is a rehabilitation technique that stimulates the peroneal nerve to restore normal movement. However, existing FES devices often lack precise charge balancing and timing accuracy, which can cause patient discomfort and potential tissue damage. To address these challenges, we developed a wearable, compact, and AI-driven FES system capable of generating biphasic, charge-balanced, trapezoidal pulses. The system integrates an ESP32 microcontroller, an OPA452-based stimulation circuit, and machine learning algorithms for foot lift detection. Unlike traditional threshold-based detection methods, our AI-enhanced approach adapts stimulation timing in real-time, improving synchronization with the patient's gait. Initial testing demonstrated the system's ability to generate precise charge-balanced stimulation pulses while accurately detecting foot-lift events. The AI-based detection method improved timing accuracy, reducing unwanted stimulation and enhancing patient comfort. The proposed system offers a technological advancement in neurorehabilitation, addressing key limitations of existing FES solutions. By integrating machine learning with FES, this work introduces a personalized, intelligent stimulation system that enhances rehabilitation outcomes for individuals with foot drop. The developed FES system achieved an average accuracy of 92.2%. Stimulation was found to be smooth between 120-220 microseconds of pulse width and 25-35 Hz of frequency.



Clustering in asynchronous distributed transmission for IoT applications A Gupta, S Agarwal - IEEE Communications Letters, 2025

Abstract: Asynchronous distributed transmission (ADT) supports scalable, energy-efficient Internet of Things (IoT) communication but suffers from time, frequency, and phase offsets at the receiver. Bit error rate (BER) performance in ADT depends on the frequency offsets between the transmitting nodes, making it a suitable parameter for system design. Motivated by this, we propose a clustering framework that groups IoT devices into a fixed number of transmitters in ADT with high intra-cluster frequency diversity to enhance BER performance. We model the clustering as a constrained combinatorial optimization problem, which is NP-hard, and solve it by proposing a Frequency-Aware Size-Constrained (FASC) clustering algorithm. FASC achieves near-optimal performance with reduced computational cost and consistently outperforms state-of-the-art schemes in terms of BER and convergence, making it well-suited for real-world ADT-based IoT systems.

Comprehensive stability analysis of fully transparent low-power thin-film transistors: Role of device design and electrical parameters

MS Mehrolia, A Verma, AK Singh - IEEE Journal on Flexible Electronics, 2025

Abstract: This article states the simulation of a-IGZO (amorphous-indium gallium zinc oxide)-based thin film transistor (TFT) using the Silvaco-Atlas tool, which is operated at a low voltage of 1.5 V. In this TFT, ZrO2 (zirconium dioxide) acts as a gate dielectric, and IZO (indium zinc oxide) is utilized as electrodes for the gate, source, and drain terminal. This simulated TFT exhibits excellent performance parameters such as a small threshold voltage (VTH) of 0.21 V, mobility (μ n) of ~ 8.37 cm2/V - s, a subthreshold swing (SS) of ~ 84 mV/decade, and a high on-off ratio ~ 106. In addition to the estimation of performance parameters, the hysteresis curve is also evaluated for gate-source voltage (VGS), which varies from 0 to 1.5 V and the same in the reverse manner. The impact of different parameters, such as variable thickness of the dielectric layer, active layer, and different magnitudes of fixed charge density, is also observed in the plotting of the hysteresis curve and in the calculation of Δ VTH. From all the cases, it has been concluded that for an oxide thickness of 40 nm and an active layer thickness of 30 nm, the change is very small in Δ VTH, that

22.

is, 0.0003, 0.0015, 0.003, "0.006," "0.009," "0.016," and "0.023 V" for stress times of "0 s," "600 s," "1200 s," "1800 s," "3600 s," "5400 s," and "7200 s." The minimal variations in threshold voltage across different stress durations confirm the enhanced positive bias stress (PBS) stability of the a-IGZO low-voltage TFT device, highlighting its potential for future low-power and flexible electronic applications.

Concentration-dependent diffusion effects on miscible radial viscous fingering L Palodhi, M Mishra - Physics of Fluids, 2025

Abstract: Radial flows, characterized by their inherent radial and tangential velocity components, present unique hydrodynamic behavior compared to unidirectional rectilinear flows. One such phenomenon is the miscible viscous fingering (VF) instability, which arises when a less viscous fluid displaces a more viscous one. In this study, we investigate the development of VF in radial geometries with a particular focus on understanding the influence of concentration-dependent diffusion coefficients. Using direct numerical simulations, we systematically explore how varying the diffusivity as a function of solute concentration affects the growth and morphology of viscous fingers. Our results reveal distinct differences in the evolution of fingering patterns when compared with the classical constant diffusivity case. We find that finger length tends to increase due to enhanced diffusion near the interface, suggesting that diffusion acts to promote the penetration of the less viscous fluid into the more viscous one. In contrast, the finger width appears to be primarily governed by advective dynamics, which dominate in the radial spreading regime. Moreover, our simulations indicate that, similar to the constant diffusion case, variable diffusivities in radial VF systems also evolve toward a characteristic pattern geometry determined by key fluid properties, such as the logarithmic viscosity ratio, R, and the functional form of the concentration-dependent diffusivity.

Cu (I)-Functionalized n-rich covalent triazine framework for integrated capture and conversion of co₂ from dilute gas into bioactive 2-oxazolidinones

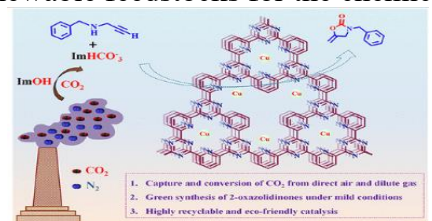
R Kishan, P Rani, S Kumar, CM Nagaraja - Energy & Fuels, 2025

24.

25.

26.

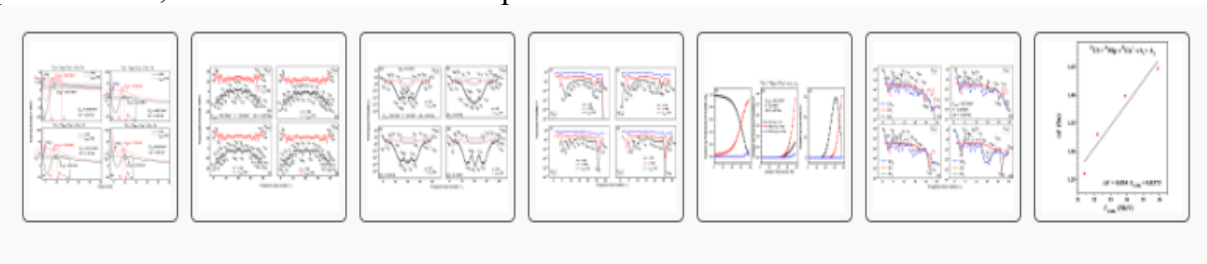
Abstract: Carbon capture and utilization (CCU) presents a promising approach for alleviating atmospheric CO₂ concentrations and yielding commodity products. In this direction, we have prepared a N-enriched and CO₂-philic pyridine-based covalent triazine framework (DCP-CTF), which is covalently anchored with Cu(I) to yield Cu(I)@DCP-CTF for effective CCU from dilute gas (15% CO₂) in the presence of ionic liquid (IL). Herein, the application of hydroxylfunctionalized IL facilitates carbon dioxide capture, and the presence of Cu(I)-embedded CTF catalyzes the transformation of the captured CO₂ into bioactive oxazolidinones. Indeed, the Cu(I) anchored CTF exhibited exceptional catalytic activity for the conversion of simulated dry flue gas (CO₂:N₂ = 15:85%) into oxazolidinones, which are valuable arbitrates in pharmaceuticals, agrochemicals, and fine chemicals. Furthermore, Cu(I)@DCP-CTF exhibited significant CO₂philicity, with an interaction enthalpy of 44.3 kJ/mol, attributed to the presence of adequate basic N-sites. The combined benefits of efficient CO₂ enrichment due to the ionic liquid and Cu(I) endowed DCP-CTF with exceptional catalytic performance and durability, positioning it as a highly promising system for sustainable CO₂ conversion under ambient conditions. Hence, this work presents a promising approach for an integrated process of selective capture and conversion of CO₂ for the production of renewable feedstocks for the chemical industry.



Decay analysis of the isotopic chain of compound nuclei 58–61Cu* formed in the reactions 35Cl +23–26Mg

N Kaur, M Kaur, A Kaur, S Kaur, S Singh, BB Singh - Physical Review C, 2025

Abstract: The neutron content of compound nuclei (CN), formed in low-energy nuclear reactions, manifests itself in the magnitude of the fragment cross sections. These days, the study of the dependence of associated decay channels on the neutron content is an attractive topic due to the worldwide availability of radioactive ion beams. The dynamical cluster-decay model (DCM) is used to analyze the decay of an isotopic chain of CN 58-61Cu*, formed in the reactions 35Cl+23-26Mg, respectively, at different center-of-mass energies Ec.m.. The DCM's collective clusterization approach, based on quantum mechanical fragmentation theory, is employed to understand the influence of successive neutron addition on the decay modes of these CN into light particles (LPs; $A \le 4$), intermediate mass fragments (IMFs; with $5 \le A \le 20$), and symmetric mass fragments [SMFs; $(ACN[\times]/2)\pm10$], and the mutual competition between them. We see that adding a neutron changes the potential energy surfaces (PESs), and, consequently, the preformation profiles of the CN change significantly from 58Cu* to 61Cu*. The PESs for all the CN show that LPs remain dominant in the decay process with their highly minimized values at all the angular momentum ℓ values, with IMFs following closely, particularly light IMFs (LIMFs; $5 \le A \le 12$). The combined results of the preformation and penetration processes yield fusion cross-section values for the given decays of LPs, IMFs, and SMFs. We find that LPs and LIMFs are the most significant decay modes, with the former being chased by the latter consistently with the successive addition of a neutron in CN from 58Cu* to 60Cu* and superseding it for the compound nucleus 61Cu*. The DCM-calculated fusion cross sections σ DCMfus are given by the sum of LP cross sections (σ LP) and LIMF cross sections (σ LIMF), which are in good comparison with the given experimental data. It is important to mention here that $\Delta \stackrel{\sim}{\times} R$, associated with the barrier-lowering phenomenon, shows a linear relationship with the Ec.m. values.



<u>Direct processing of biomass using high-power blue laser</u>
JS Devara, BK Dadhich...**R Ahuja**, KP Singh - Advanced Sustainable Systems, 2025

27.

28.

Abstract: Inventing new approaches to transform abundant plant matter swiftly into valuable products is crucial for sustainable development. Here, the first direct and continuous conversion of lignocellulosic solid mass into synthetic biogas is reported using blue laser irradiation at multi-kW/cm² intensity. It is demonstrated that the on-demand generation of a biogas jet, achieving rapid (in milliseconds) and continuous production of a flame jet 300 times larger than the mm-size laser focus. Remarkably, biogas production occurs exclusively during laser illumination, without triggering bulk combustion, and achieves up to 92% mass conversion. A comprehensive phase diagram of the blue light—wood interaction highlighting three distinct regimes accessed is reported by varying laser parameters and provide mechanistic insight using photothermal simulations. Furthermore, the molecular composition of the synthetic biogas is identified and is shown to result from the photothermal decomposition of lignocellulose molecules. The biogas, collected independently, is shown to produce a sustained flame. Successful bio-gasification of 16 kinds of woods proves that the all-optical approach is solvent-free, non-contact, scalable, and universally applicable.

Disordered open plasmonic cavities for broadband emission enhancement of nitrogen-vacancy center

N Singh, H Sammi, N Ahmed, N Sardana, RV Nair - Advanced Optica Materials, 2025

Abstract: The unique optical and spin properties of nitrogen-vacancy (NV) centers have revolutionized the possibilities of room-temperature quantum technologies. However, the applicability of NVs can be further enhanced by coupling them with plasmonic structures. Here, the integration of a few NVs is discussed with disordered open plasmonic cavities made of gold for broadband emission enhancement at room temperature. The study involves a statistical analysis of coupled NVs, revealing accelerated emission rates and enhanced intensity with scalability, long-term stability, and reproducible emission properties. The disordered open cavities enhance the spontaneous emission decay rate by a factor of five by enhancing the local density of optical states, supported by numerical simulations. The extent of enhancement depends on the spatial variation in nanopore size, affecting mode volume in the proximity of NVs. The statistical variation in the estimated pore size is directly related to the measured lifetime distribution, implying the robustness of the disordered sample over a large area with strong emitter-cavity coupling. The results are useful to enhance the sensitivity of NV-based quantum sensors and to realize bright single-photon sources. The structure is also suitable for many other quantum emitters with slow emission rates and for developing room-temperature quantum technologies.

Dynamic interactions of geopolitical risk, economic policy uncertainty and market volatility with stock and commodity markets: Evidence from India

B Raina, S Bardhan - International Economic Journal, 2025

Abstract: This study examines the dynamic interactions of Geopolitical Risk (GPR), Economic Policy Uncertainty (EPU), and the Volatility Index (VIX), with financial and commodity markets in India by incorporating both global and India-specific GPR measures, alongside EPU-India and India-VIX indices. Using the wavelet coherence and DCC-GARCH (1,1) models on monthly data from January 2000 to December 2023, the study investigates co-movements and lead-lag relationships between uncertainty indicators and stock markets, precious metals, and crude oil. Findings reveal that the effects of uncertainty shocks on stock and commodity markets are timevarying and frequency dependent. Among the uncertainty measures, India-VIX and EPU-India exert strong, persistent negative effects on the BSE-500 over medium and long-term horizons. India-GPR exhibits mostly positive, short-lived co-movements with the BSE-500, while World-GPR linkages remain weak. Unlike silver, gold demonstrates robust hedging properties against India-VIX, while its co-movements with EPU-India and GPR are asymmetric and event-specific. Crude oil displays positive long-term co-movements with GPR and persistent negative patterns with EPU-India and India-VIX. Findings seem to be relevant to investors while designing portfolios and risk management strategies, and to the policy makers as well while framing appropriate policies in anticipating market reactions and forming market expectations, respectively.

Dynamics of Portevin-Le Chatelier banding revealed through grain refinement in high-Mn austenitic steel: sequential overcoming of necking

S Hwang... A Lavakumar... A Shibata... - Journal of Materials Science & Technology, 2025

Abstract: Dynamics of Portevin-Le Chatelier (PLC) banding were thoroughly revealed through grain refinement in high-Mn austenitic steel. Fully recrystallized 22Mn-0.6C steels (wt%), with mean grain sizes ranging from 8.4 μm (coarse grain, CG) to 0.82 μm (ultrafine grain, UFG), were successfully fabricated through repeated cold rolling and subsequent annealing. Serrations were observed on the global stress-strain curves of all specimens, while the UFG specimen showed notably weak serrations in the early stages of deformation. Using the digital image correlation (DIC) technique, the serration behavior on the stress-strain curves of all specimens was found to perfectly correspond to the local heterogeneous deformation characterized by the formation, propagation, and annihilation of PLC bands. With grain refinement, localized deformation within the PLC band decreased, while the deformation beyond it became more pronounced, resulting in more homogeneous deformation across the entire gage part. This study presents the first experimental evaluation of the local strain-hardening rate through the simultaneous application of in-situ synchrotron XRD and DIC measurements during the tensile test. It was found that necking was periodically triggered but was soon overcome through the high strain hardening within the propagating PLC bands, which was achieved through the localized multiplication of dislocations and the formation of stacking faults. The UFG specimen exhibited greater local strain hardening than the CG specimen, induced by the formation of more dislocations and stacking faults. Such an increase in local strain hardening with grain refinement resulted in more homogeneous deformation behavior and consequently weaker serrations in the early stages of deformation.

Effect of bacillus megaterium on the strength and microstructure of concrete at different curing ages and bacterial concentrations

A Shukla, N Gupta, K Kishore - Innovative Infrastructure Solutions, 2025

Abstract: This study investigates the use of Bacillus megaterium, an alkali-resistant, calcite-precipitating bacterium, to enhance the mechanical performance of concrete. Bacterial strains were isolated and introduced into the cement concrete mix at concentrations of 10⁶, 10⁷, and 10⁸ cfu/mL. The bacteria, known for high urease activity, facilitated the precipitation of calcium carbonate (CaCO₃) in the form of calcite, contributing to crack healing and matrix densification. Concrete specimens were tested for compressive, tensile, and flexural strength at 7, 28, 56, 90, and 180 days of curing. Microstructural characterization was conducted using scanning electron microscopy (SEM) and energy dispersive X-ray spectroscopy (EDS). Results showed an increase of up to 15% in compressive strength compared to control specimens, with the 10⁷ cfu/mL concentration yielding the most significant and consistent improvements. The SEM and EDS confirmed dense microstructures and increased Ca and O content in bacterial concrete. Compared to earlier studies, this research highlights the importance of optimizing bacterial concentration to maximize performance. The findings underscore the potential of microbial concrete to enhance durability, reduce cement usage, and contribute to environmentally sustainable construction practices.

31.

Effects of perceived safety gain, satisfaction, and benefits on autonomous vehicle preferences for long-distance discretionary trips in India

TM Rahul, Nikhil - Transportation Research Part F: Traffic Psychology and Behaviour, 2025

Abstract: Fully autonomous vehicles (FAVs) can have a significant impact on the travel demand for long-distance discretionary travel. With its diverse culture and weather, and numerous tourist destinations, India has a huge potential for long-distance discretionary travel (LDDT). The current study models the respondent's willingness to travel more and longer for long-distance discretionary trips in FAVs. Integrated Choice Latent Variable (ICLV) models that incorporate psychological constructs are used for estimation. Structural equations that capture the mediating effect of perceived satisfaction on the causal relationship between perceived benefits and willingness are formulated. Consistent with ambiguity aversion and familiarity effect theory, a novel predictor that represents the relative safety perception of FAVs compared with partial autonomous vehicles (PAVs) is introduced in the utility function of the choice model. The data for empirical analysis were obtained from the city of Chandigarh, India. The results elicited a strong indirect effect for perceived benefits on the decision of an individual to travel more and longer in FAVs with perceived satisfaction acting as the mediator variable. Supportive infrastructure, and a clear and well-defined cyber security framework improved the willingness among people to use FAVs for long-distance travel. From an equity perspective, FAVs were found to enhance the mobility of transport disadvantaged groups which included females and older adults.

Enhancing medication adherence in drug-resistant epilepsy using "Epilepto": A pilot randomized controlled trial (EMPOWER-E)

P Tewari, S Agarwal, L Saini, S Manjunathan, R Shukla, RS Krishnu, VP Nathasha, A Shahani, K Singh... - Epileptic Diorders, 2025

Abstract: Objective: Drug-resistant epilepsy is a disabling, chronic condition in children. Longterm prognosis depends on the extent of seizure control. Ensuring compliance with medication can help reduce the seizure burden. Forgetfulness is a key barrier to adherence. To address this, we used a mobile application, "Epilepto," to deliver regular medication reminders aimed at improving compliance. Method: We enrolled children with drug-resistant epilepsy aged 3 months to 18 years with varied etiology and randomized them into two groups. The intervention group was trained to use the application to help remind them of the medications, along with the standard of care treatment given to the control group. Medication adherence was assessed using the Morisky Medication Adherence Scale-8 (MMAS-8), and seizure burden was assessed using the Early Childhood Epilepsy Severity Scale (E-Chess). All the children were assessed at 3 and 6 months after enrolment. Results: A total of 100 children were randomized (1:1) to either the control or intervention group. The median age of children in the intervention group was 84 months (Interquartile range, 45–144), and the control group was 96 months (48–144). Overall, 70% of the children were boys, and 52% had generalized epilepsy. The majority of the cases had a structural (70%) or a genetic (20.6%) etiology. Most of the users found daily reminders useful (42/48). 81.2% found this an acceptable intervention at the 6-month follow-up. There was a gradual improvement in the MMAS-8 scores over 6 months, with a 30% rise in high adherence in the intervention group as compared to only a 6% rise in the control group. There was no reduction in seizure burden as assessed by E-Chess at the end of the study period. Significance: The use of medication reminders appeared to be a feasible intervention for children with drug-resistant epilepsy to improve medication adherence. Key points: Medication adherence is important to achieve seizure control in children with drug-resistant epilepsy. Use of the mobile application (Epilepto) helped caregivers achieve better medication adherence over a period of 6 months. Despite improved medication adherence, seizure control did not improve, likely due to the resistant nature of the disease and the pilot study design.

32.

F18 promiscuous epitope of acr1 protein of mycobacterium tuberculosis induces the secretion of IL-10 and tregs but not IL-6

T Lamba, S Prajapati, A Chowdhury, A Bandyopadhyay, JN Agrewala - Protein & Peptide Letters, 2025

Abstract: Introduction: italic>Mycobacterium tuberculosis (Mtb) is a Gram-positive bacterium that causes tuberculosis (TB). It remains viable for extended periods within host macrophages by entering a dormant state. Alpha crystallin 1 (Acr1) is a 16 kDa protein of Mtb and is reported to be highly upregulated in latent TB. Acr1 suppresses the host's immune system by impairing the differentiation and maturation of dendritic cells and macrophages. We hypothesize that Mtb judiciously utilizes its Acr1 protein to paralyse the immune system of the host by inducing the release of IL-10 and generating an immunosuppressive environment. Methods: We employed in silico tools to identify highly promiscuous, IL-10-inducing and IL-6-non-inducing epitopes of Mtb. Moreover, the selected epitope was synthesized and tested for its suppressive activity and generation of Tregs. Results: We identified the presence of a specific epitope in Acr1 (F18) that is responsible for bolstering the release of IL-10 and Tregs through in silico tools and verified the activity by in vitro assays. In hPBMCs, the F18 epitope could suppress the proliferation of CD4 T cells stimulated with PHA and expand the pool of Tregs in a dose-dependent manner. Discussion: The F18 epitope from Mtb's Acr1 protein promotes IL-10 and Treg responses without triggering pro-inflammatory IL-6, suggesting its probable immunoregulatory role. While it holds potential for treating autoimmune diseases, its impact on infection in tuberculosis should be further investigated. Conclusion: Our findings suggest that the F18 epitope induces IL-10 production and Treg differentiation while inhibiting CD4⁺T cell proliferation and IL-6 secretion, thereby promoting an immunosuppressive environment. Furthermore, this study highlights the possible role of Acr1 and its immunosuppressive epitope F18 as therapeutic agents for inducing suppressive Tregs, which may help in the management of autoimmune diseases.

Firm investment, financial constraints and agency costs: evidence from India MA Vincent, PK Das, S Bardhan - Empirical Economics, 2025

Abstract: The investment slowdown among Indian firms is a pressing concern with far-reaching implications for the nation's growth trajectory. Against this backdrop, the present study investigates how finance constraints and agency costs impact firm-level investment efficiency. Based on the Prowess database of Indian private manufacturing firms between 1999 and 2024, we employ two-tier stochastic frontier model (2TSFM) with intra-error dependence to analyse investment inefficiencies arising from under-investment (due to finance constraints) and over-investment (due to agency costs). Our results reveal a significantly negative association between finance constraints and investment, and a significantly positive association between agency costs and investment. Firms with lower agency costs face lesser finance constraints, enabling them to invest more; however, as agency costs increase, this positive effect diminishes, indicating that even some firms with high agency costs still manage to secure external funding. These findings highlight the need for targeted reforms in firm financing and corporate governance to enhance investment efficiency and foster sustained economic growth in emerging economies such as India.

Granular ball twin support vector machine with Universum data MA Ganaie, V Ahire - Neural Networks, 2025

Abstract: Support vector machines often underperform when limited to labelled target class data and demonstrate sensitivity to noise and outliers. To address these limitations, we propose the Granular Ball Twin Support Vector Machine with Universum Data (GBU-TSVM), which uniquely integrates Universum samples with granular ball computing in the TSVM framework. Unlike conventional TSVMs representing data as points in feature space, the proposed GBU-TSVM models instances as hyperballs, significantly improving robustness against noise while enhancing computational efficiency. Granular representation enables effective data grouping, reducing processing complexity while preserving critical structural information. Incorporating Universum data, consisting of samples outside the target classes, provides additional contextual information

34.

35.

that refines decision boundaries and improves generalization. Experiments on UCI benchmark datasets demonstrate GBU-TSVM's superior performance, measured in terms of accuracy and training time. It achieves 92.38 % accuracy on the Molec Biol Promoter dataset under optimal conditions and maintains 89.17 % accuracy even with 20 % noise contamination. It consistently outperforms baseline models such as GBSVM, TSVM, GBTSVM, Pin-GTSVM, and UTSVM. These results establish GBU-TSVM as an advanced framework for robust classification in challenging data environments.

<u>Hemodynamics and heat transfer in bifurcated blood vessels: Insights from a two-phase Eulerian-granular model on bifurcation angle and asymmetry effects</u>

SS Das, SS Banerjee, C Sasmal - International Journal of Thermal Sciences, 2025

Abstract: Understanding the influence of geometrical configurations on blood flow and heat transfer is essential for vascular physiology and biomedical applications, such as in the thermal ablation process to destroy tumour cells. This study presents an extensive numerical investigation of the impact of bifurcation angle (Ω_{bif}) and asymmetry on hemodynamics and thermal transport in three-dimensional bifurcated arteries under realistic physiological pulsatile flow conditions. An Eulerian-granular two-phase model, incorporating the kinetic theory to account for red blood cell (RBC) particle mechanics, is employed in the present simulations. By incorporating particle mechanisms, the present model provides better predictive capabilities compared to single-phase Newtonian, non-Newtonian, and two-phase Euler-Euler models, showing better agreement with experimental data. The results indicate that increasing the bifurcation angle reduces blood velocity at the inlet of branch vessels, subsequently diminishing the heat sink effect due to a decrease in convective cooling. For symmetric configurations, RBC concentration near the inner walls of branch vessels decreases with increasing Ω_{bif} , whereas for asymmetric configurations, RBC accumulation near the inner wall increases relative to the outer wall. A persistent thermal gradient between the inner and outer walls leads to differential heat dissipation, affecting local tissue cooling during thermal therapies. These findings of the present study highlight the critical role of vascular geometry in regulating hemodynamic and thermal interactions, with potential implications for cardiovascular diagnostics, vascular graft design, and targeted therapeutic applications.

Immediate and delayed side effects of irreversible electroporation on epidermal keratinocytes **B Das**, F Berthiaume, A Shrirao, R Schloss... - Bioelectricity, 2025

Abstract: Irreversible electroporation (IRE) has been explored significantly for health care applications, especially cancer therapy and wound healing. It is associated with massive cell death via the bursting of cells caused by the creation of nanopores due to the rapid alteration of a voltage gradient across the cell membrane. It is reported to disinfect chronic wounds and burn injuries, minimize scar tissue formation, and regenerate accessory organs like hair follicles. However, several theories surround this therapy's efficacy, such as the activation of immune pathways via paracrine secretion. The current study used a keratinocyte cell line (HaCaT) monolayer as an in vitro model to explore the significant immediate side effects of applying IRE. IRE was applied to cellular monolayers via needle electrodes as bursts of pulsed electric field (PEF). We observed via microscopic image analysis that there were input voltage-dependent alterations in cellular monolayer morphology visible in both phase contrast and using fluorescent live/dead staining. Similar changes were observed in reactive oxygen species-specific staining, mitochondrial membrane potential-specific staining, and cell membrane lipid peroxidation-specific staining. All the micrographic imaging showed that the affected area was highly correlated with the input voltage. Furthermore, a multiphysics simulation of the IRE applied to the cellular monolayer for an individual pulse was performed to characterize the electric field intensity spatial distribution. It exhibited similarities with the morphological alteration profiles in the cellular monolayer post-PEF application. We also found multinucleated or fused cells outside the IRE-induced immediate death zone, which could also be another side effect of this exposure.

38.

Impact of interface traps and fixed interface charges on polarization and TER ratio in MFIS ferroelectric tunnel junctions: A TCAD study

A Kumar, T Ali, D Lehninger, P Duhan - Journal of Applied Physics, 2025

Abstract: Hafnium dioxide (HfO 2)-based ferroelectric tunnel junctions (FTJs) have the potential to dominate the next generation non-volatile memories and neuromorphic computing applications. These devices have been found to be promising memory devices due to their non-destructive readout, CMOS compatibility, and cost-effectiveness. However, the presence of charge trapping/de-trapping and fixed charges can be challenging for read/write operations as they can alter the polarization and cause device variability. This work primarily focuses on the impact of interface traps and fixed charges on the performance of metal-ferroelectric-insulator-semiconductor-based FTJs using technology computer-aided design simulations. This study comprises donor- and acceptor-type traps at the interface of silicon/silicon dioxide (Si / SiO 2) and fixed charges (positive and negative) at the SiO 2 / HfO 2 interface. As indicated by the simulation results, the interface states impact the depolarization field (E d) and remanent polarization (P r). This eventually affects the read current density (J) and varies the tunneling electro resistance (TER) ratio of the FTJ devices. A comprehensive analysis of the individual and combined effects of interface traps and fixed interface charges highlights their critical role in determining key FTJ performance metrics.

<u>Influence of non-planar orientations on solidification microstructure during robot-assisted laser-wire directed energy deposition</u>

S Rathor, DK Goyal, **R Kant**, **E Singla** - CIRP Journal of Manufacturing Science and Technology, 2025

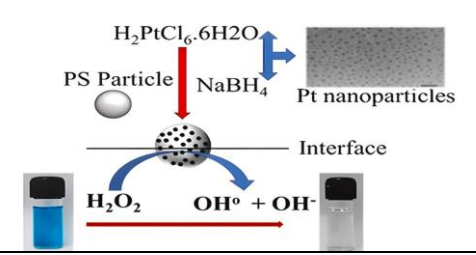
Abstract: This work investigates the effect of temperature gradient on the solidification morphology during the non-planar laser-wire directed energy deposition (LWDED) process, abbreviated as DED-LB/w according to ISO/ASTM 52900:2021 standard. The LWDED abbreviation is used further in this work. The novelty of this study lies in the independent variation of substrate tilt angle (STA) and wire feed angle (WFA), which presents a comprehensive understanding of non-planar depositions. The temperature distribution and solidification parameters were computed using a customized 3D transient heat transfer model. This numerical model was introduced considering the pulsed laser beam, laser spot shape and size change due to different non-planar orientations. Solidification time, microstructural changes, and heat-affected zone (HAZ) morphology were discussed by correlating the stainless steel 316 L temperature distributions. A numerical and experimental analysis was presented for single-layer deposits. The STA and WFA significantly influence the cooling rates during solidification, affecting the microstructure of the beads. Lower STA (0°-15°) and WFA (10°-20°) result in higher cooling rates. The change in the laser beam spot size affects the solidification rate in the tilt direction due to the lower heating concentration. Smaller WFA (10°-20°) enables the wire to be positioned closer to the molten pool. It results in better energy absorption and efficient melting by increasing temperature. It increased the initial temperature difference and cooling rate. The fraction of equiaxed solidification morphology from the centre to the tilt direction increased with a reduced thermal gradient. The main outcome of this work is the validated solidification map for non-planar LWDED for optimizing deposition strategies in supportless additive manufacturing. The present approach will help suggest the deposition orientations to achieve consistent quality and reliability in deposited parts at non-planar orientations. This work is required to decide deposition strategies for supportless additive manufacturing.

40.

Interfacial engineering approach for enhanced degradation of methylene blue using platinum-coated polystyrene rough particles: Flow-regulated catalytic activity and kinetic modeling

F Khan, VS Pawak, C Shekhar, VR Dugyala, T Mondal, M Sabapathy - Case Studies in Chemical and Environmental Engineering, 2025

Abstract: This study explores an efficient decontamination strategy using platinum-coated polystyrene rough-particles as a micron-sized catalyst system for decomposing methylene blue (MB), a common organic pollutant. The synthesized nanomaterials were comprehensively characterized using Nanoparticle Tracking Analysis (NTA), Dynamic Light Scattering (DLS), Atomic Force Microscopy (AFM), Scanning Electron Microscopy (SEM), and Transmission Electron Microscopy (TEM), confirming their morphology, size distribution, and surface properties. The decontamination was performed at the air-water interface through an interface trapping method, with enhanced mixing achieved under a controlled flow environment. The experiments were conducted with a circulation speed of 50 RPM, corresponding to a Reynolds number (NR_e) of 1686 and a high particle packing fraction of 0.8. Under these operating conditions, complete degradation of MB was achieved within 30 min, significantly faster than the 75 min required for degradation in the bulk phase. The reaction kinetics were analyzed and found to follow the Langmuir-Hinshelwood model, with an estimated rate constant of 0.018 min⁻¹, indicating efficient surface-mediated catalytic activity. Furthermore, an Artificial Neural Network (ANN) model was developed to validate and predict the degradation kinetics, showing a Root Mean Square Error (RMSE) of 5.5 and a high correlation coefficient (R²) of 0.9656, confirming the reliability of the predictive model. This interface-assisted, catalyst-based degradation approach demonstrates a promising, reusable, cost-effective, and environmentally friendly solution for advanced wastewater treatment applications.



Inverse problem for a time-dependent convection—diffusion equation in admissible geometries: RK Mishra et al.

RK Mishra, A Purohit, M Vashisth - Research in the Mathematical Sciences, 2025

Abstract. We consider a partial data inverse problem for a time-dependent convection-diffusion equation on an admissible manifold. We prove that the time-dependent convection term and time-dependent density can be recovered uniquely modulo a known gauge invariance. There have been several works on inverse problems related to the steady state convection-diffusion operator in Euclidean as well as in Riemannian geometry settings; however, inverse problems related to time-dependent convection-diffusion equation on a manifold are not studied in the prior works, which is the main aim of this paper. In fact, to the best of our knowledge, the problem studied here is the first work related to a partial data inverse problem for recovering both first and zeroth-order time-dependent perturbations of evolution equations in the Riemannian geometry setting.

Long life with ultrahigh capacitance flexible electrode at practical mass loading for battery supercapacitor hybrid

M Singh, A Kafle, D Gupta, TC Nagaiah - Small, 2025

41.

43. **Abstract:** Designing economic and bio-degradable flexible electrodes with industry-standard mass loading (>10 mg cm⁻²) poses significant challenges for stable and durable energy storage devices. In this report, an endeavor is made to design flexible and bio-degradable laboratory filter paper-based electrodes for eco-friendly and pocket-friendly flexible battery supercapacitor hybrids (BSHs) via a combination of electroless and electrodeposition techniques. Filter paper (FP) is

made conductive by electroless deposition of NiB-layer (Ni/NiB-FP) on which high mass loadings of nickel iron phosphide active material (4.5 to 17 mg cm⁻²) are deposited via electrodeposition method for the development of NiFeP@Ni/NiB-FP flexible electrodes. The developed NiFeP@Ni/NiB-FP electrode (17 mg cm⁻²) undergoes electrochemical activation by surface reconstruction to achieve ultrahigh areal capacitance of 37.5 F cm⁻² (18.75 C cm⁻², 2220 F g⁻¹) at 5 mA cm⁻² as battery type electrode with exceptional rate capability (90.6% at 30 mA cm⁻²) and ultrastable cycling retaining 37.4 F cm⁻² at 5 mA cm⁻² even after continuous cycling for 1329 h (≈55 days). As a proof of concept, a tandem device with four flexible paper-based BSH cells in series is demonstrated to achieve stable operational voltage up to 6 V. Practical applicability is showcased by powering a panel with 50 LEDs (each rated 1.6 V), a small fan, a digital calculator and a digital thermometer while measuring the body temperature highlighting the versatility for for diverse applications.

Mechanistic insights into surface tension reduction: The potential contribution of nanobubbles K Agarwal, N Dutta, N Nirmalkar - Journal of Molecular Liquids, 2025

Abstract: It is currently pure conjecture as to whether bulk nanobubbles (BNBs) can lower a liquid's surface tension. In the present study, we propose a hypothesis that aims at identifying the underlying mechanism. Here, nanobubbles are probably governed by the diffusion-limited adsorption model, assuming that surface excess near the interface causes the emergence of an instantaneous equilibrium state. The minuscule time constraint for the nanobubble uptake at the free surface is ruled out by applying the asymptotic limit for the dynamic interfacial tension where t and the net reduction in surface tension (), is directly proportional to the concentration of nanobubbles (C_{NB}) and inversely proportional to the diameter of the nanobubbles (D_{NB}). Nanobubbles were generated by coupling the pathway of the compression-decompression technique and salting-out effect. For all cases, surface tension was estimated and subsequently correlated with the nanobubble properties, and a mechanism was proposed that elucidates a sudden drop in the surface tension at certain salt concentration ranges. It was observed that the sudden decrease in the surface tension was fostered by the presence of charged nanobubbles, likely to be adsorbed on the free surface along with the electrostatic attractive force, both presumably responsible for the surface excess. The presence of a gaseous nanoscale domain has been confirmed by atomic force microscopic (AFM) images depicting the bubble diameter approximately consistent with the mean size measured through nanoparticle tracking analysis (NTA).

Metathesis-synthesized [BMIM][HPO₄]: Physicochemical and electrochemical characterization for supercapacitor applications

AN Rao, P Kumar...L Bainsla - Chemistry Select, 2025

Abstract: Ionic liquids (ILs) are widely recognized for their high thermal and electrochemical stability, making them promising candidates for integration into batteries and supercapacitors (SCs). In this study, an IL synthesized from BMIMCl and disodium hydrogen orthophosphate through a metathesis approach shows exceptional thermal stability up to 618 °C. Comprehensive electrochemical tests are conducted using activated carbon-based electrodes to assess their potential in SC applications. Detailed physicochemical characterization is also performed. The synthesized IL demonstrates a 2.2 V electrochemical stability window, a specific capacitance of 91.6 F/g, a power density of 1.8.47 kW/kg at a current density of 1 A/g, and an energy density of 61.57 Wh/kg.

Morphometric analysis of sand mining-induced changes in the Sutlej River S Kaur, A Gani, S Pathak, **RK Tiwari** - Environmental Geochemistry and Health, 2025

Abstract: The fluvial morphology of rivers is highly dynamic and vulnerable to both natural processes and human interventions. This study presents a comprehensive morphological assessment of the Sutlej River in the Jalandhar region of Punjab, India, with a particular focus on the impacts of sand mining. Geomorphic indicators, including river migration, channel width, bank erosion, and bar dynamics were determined by using multi-temporal satellite imagery for the year 2014 and 2024 with respect to the year 2001. Significant temporal and regional differences in channel morphology were found by the investigation, especially at sites where sand mining is heavily practiced. A detailed geomorphometric evaluation of the basin was conducted using SRTM-derived DEMs and standard hydrological tools, revealing a dendritic drainage pattern and moderate drainage texture (4.95), indicative of relatively stable fluvial conditions. Pronounced lateral shifts were observed in proximity to 35 identified sand mining locations, as evidenced through riverbank delineation and displacement analysis conducted at 5 km intervals. Comparative assessments of sediment load between post-monsoon 2023 and pre-monsoon 2024 further highlighted sediment redistribution associated with intensive mining hotspots. The results underscored the changed sediment transport patterns, accelerated channel dynamics due to sand mining and made areas more susceptible to flooding and ecosystem loss. The findings demonstrate a clear spatial association between intensified mining activity and increased bank erosion. The lateral shift of banks in varied from 8.6 to 972.49 m, whereas the total deposition and erosion area at both the banks was determined as 1561.85 ha and 2263.41 ha respectively. The total deposited area in the study area at left and right bank was 637.65 and 924.20 ha respectively, whereas the total eroded area at left and right bank was 1247.17 and 1016.24 ha. In addition to being a sign of geomorphic instability, these changes present significant threats to the riverine ecosystem, such as habitat loss, decreased sediment connection, and heightened vulnerability to flooding. The findings underscore the urgent need for sustainable sand mining practices, reinforced by continuous geomorphological monitoring using GIS and remote sensing, to mitigate environmental impacts and support effective management of riverine ecosystems.

Nonlinear absorption of Ag2S, Ag2Se, PbS, and PbSe quantum dot-containing thick films RA Ganeev, SV Aslanov...**SR Konda**... - Optical Materials, 2025

Abstract: The nonlinear absorption properties of silver sulfide, silver selenide, lead sulfide, and lead selenide quantum dot (QD) thick films (30 μ m) were investigated using the 800 nm, 50 fs fs laser pulses. The influence of laser intensity on the nonlinear absorption coefficient on laser

45.

46.

intensity was studied to understand the competition between saturable absorption, two-photon absorption, and reverse saturable absorption. The comparison of the films and colloidal solutions of the same QDs highlighted the influence of film structure and QD interactions on the third-order nonlinear optical parameters.

Nanobubbles as a promising bacterial deactivation tool: Deactivation mechanism and ROS detection

A Das, N Nirmalkar - Journal of Environmental Management, 2025

48.

49.

Abstract: This study hypothesized that bacterial deactivation by NBs is primarily driven by oxidative damage. This damage results from the production of ROS and ORP of NBs, which depends on the type of gas they contain. To validate this hypothesis, a comparative antibacterial activity analysis of O₃-NBs, O₂-NBs, and Air-NBs was conducted on E. coli and S. aureus. The ROS and ORP levels were quantified for each type of gaseous NBs. Protein release from bacterial cells was measured as a biomarker of NBs-induced oxidative damage. FESEM was employed for the visual confirmation of the bacterial cell wall degradation. O₃-NBs achieved a 99.99% bacterial reduction within 15 min of treatment, outperforming O₂-NBs (83.89% for E. coli, 64.17% for S. aureus) and Air-NBs (79.38% for E. coli, 56.12% for S. aureus) over 60 min. The superior bacterial deactivation property of O₃-NBs was attributed to the elevated ORP and ROS generation. Oxidative damage was confirmed by protein release assays and FESEM data. These findings underscore that the antibacterial efficacy of NBs is primarily driven by their ORP and ROS generation properties, which depend on the type of gas in the NBs.

Physics informed neural network-based framework for two-dimensional phase change problems S Patra, M Agrawal, P Rath, A Bhattacharya - Computer Physics Communications, 2025

Abstract: In this work, we propose a framework to solve two-dimensional phase change problems with arbitrary shaped interfaces using physics-informed neural network. These problems are characterized by moving interfaces driven by the heat flux distribution during the phase change process. We model the phase change using a diffuse interface enthalpy formulation, where the interface has a finite width and phase change occurs over a specified temperature range. A loss function only based on the temperature field is formulated, by reframing the latent enthalpy change in terms of the temperature field and phase change temperature range. This allows us to predict the transient temperature field and interface position with the help of a simple PINN architecture consisting of a single neural network. Further the loss function does not consist of any terms related to the interface condition, making the overall implementation simple in nature. We demonstrate the effectiveness of our approach by solving a series of problems with different combinations of boundary conditions and heat sources without using any prior data and illustrate how the proposed framework can capture solution of phase change problems with arbitrary-shaped dynamic interfaces.

<u>Polarization-independent electromagnetically induced transparency in a bound state in continuum assisted terahertz metamolecule</u>

50. BK Bhowmik, LK Vaswani...**G Kumar** - Journal of Infrared, Millimeter, and Terahertz Waves, 2025

Abstract: This study numerically and experimentally demonstrates the manifestation of electromagnetically induced transparency (EIT) due to quasi-bound states in the continuum (quasi-BICs) induced by symmetry breaking in terahertz metamolecules. The metamolecule comprises four square-shaped ring resonators, exhibiting a BIC mode protected by symmetry. Under the effect of mirror symmetry breaking, the BIC mode transforms into a quasi-BIC mode, manifesting as an EIT-like window. The study indicates that the EIT response remains invariant for polarizations and various incident angles. The BIC effect arises due to the strong coupling between the bright (continuum) and dark (discrete) modes. A coupled harmonic oscillator model is proposed to understand the coupling mechanism and establish a connection between BICs, quasi-BICs, and EIT evolution. It is observed that the transmission window exhibits a significant group delay of 17 ps, highlighting the strong slow-light effect within the metamolecule. Terahertz timedomain spectroscopy (THz-TDS) is employed to experimentally measure the fabricated samples, validating the simulation and theoretical findings. This study paves the way for developing novel THz devices, such as sensors and slow-light systems, exploiting high-Q resonances for applications in terahertz photonics.

<u>Pyridine-hydrazone-based charge-transfer probe for detecting Cu2+ and Co2+ ions in aqueous</u> solutions

J Park, DI Moon, **B Shah**, **N Singh**, DO Jang - Spectrochimica Acta Part A: Molecular and Biomolecular Spectroscopy, 2025

Abstract: In the field of environmental monitoring, there remain considerable challenges regarding the development of selective chemosensors with high sensitivity for detecting transition metal ions in aqueous media. In this study, we prepared and investigated 1,3-bis((2-((E)-(2-(pyridin-2-yl)hydrazineylidene)methyl)-1H-pyrrol-1-yl)methyl) benzene as pyridinehydrazone-based probe (receptor A) for the selective detection of metal ions. Upon interacting with Cu²⁺ and Co²⁺ ions, the probe responded with significant optical changes, thereby facilitating simple ion detection. The ultraviolet-visible absorption maximum of the receptor A underwent a remarkable hypsochromic shift to 291 nm upon the addition of Cu²⁺ solution, while the addition of Co²⁺ solution led to a bathochromic shift to 426 nm. Receptor A was capable of selectively detecting Cu²⁺ and Co²⁺ in aqueous solutions without any marked interference from other metal ions, with respective limits of detection of 2.12×10^{-6} and 3.47×10^{-8} M, which are significantly lower than the WHO guidelines. The ability of receptor A to detect Cu²⁺ and Co²⁺ in real water samples was also demonstrated. These findings highlight the potential utility of pyridinehydrazones as an effective probe for real-time monitoring of Cu²⁺ and Co²⁺ ions in environmental samples.

51.

52.

Hypsochromic shift to
$$\lambda_{max}$$
 = 291 nm, colorless

$$\lambda_{max} = 330 \text{ nm},$$

Bathochromic shift to $\lambda_{max} = 426 \text{ nm},$ green-yellow

Quantum state-resolved rotational scattering of C5H+ by H2 in the interstellar medium P Chahal, TJ Dhilip Kumar - The Journal of Chemical Physics, 2025

Abstract: The interstellar medium (ISM) is a complex and dynamic environment in which molecular collisions play a crucial role. Among these, protonated carbon chains are of great interest due to the presence of a permanent dipole moment and their relevance in describing astrochemical processes, making their detection possible in cold molecular clouds such as TMC-1. C_5H^+ (1 Σ g +) is an important molecule for understanding the formation and evolution of carbon-rich environments. However, to accurately model its abundance and spectroscopic properties, it is essential to account for its collisional interactions with H₂, the most abundant molecule in the ISM. In this study, we present a quantum dynamical study for the C₅H⁺-H₂ collision, employing highlevel CCSD(T)-F12a/aug-cc-pVTZ calculations to construct an accurate potential energy surface (PES). The PES is further augmented using a neural network fitting model, ensuring spectroscopic accuracy. The PES is expanded into radial components using bispherical harmonics. Then, close coupling methods were used to calculate cross sections and rate coefficients for different rotational transitions of C₅H⁺, up to 100 K. Throughout the temperature range, a propensity is observed for even transitions over odd transitions. The rate coefficients for He and H₂ collisions are compared for C₅H⁺, C₅, and C₆H⁻. For both low and high temperatures, rate coefficients for C₅H⁺ are found to be higher than C₅ and C₆H⁻ for both the He and H₂ collisions.

Rational design of 2D2D porphyrin metal-organic nanosheet/g-C3N4 heterostructure for enhanced production of hydrogen under visible-light

S Kumar, CM Nagaraja - Journal of Colloid and Interface Science, 2025

Abstract: The development of heterojunction-based photocatalysts is a promising strategy to achieve enhanced green hydrogen (H₂) production by facilitating the competent separation of photo-induced charge carriers. In this context, two-dimensional (2D) metal-organic nanosheets (MONs) have garnered considerable attention owing to their unique properties of highly exposed active sites, ultrathin thickness, and large surface area. Especially, porphyrin-based 2D MONs have gained significant interest due to their optimum band structure and exceptional visible light harvesting properties. Herein, we efficaciously constructed a group of 2D porphyrin nanosheets (M-PNs, M = Pd, Pt, and Ni) and 2D-2D g-C₃N₄/Pd-PNs (CN-Pd) heterojunctions to achieve enhanced photocatalytic H₂ production assisted by visible light irradiation ($\lambda \ge 420$ nm). Among the 2D MONs, Pd-porphyrin nanosheet (Pd-PNs) displayed a substantially higher H₂ evolution rate (HER) of 4910 µmol g⁻¹ h⁻¹ over Pt-PNs (2490 µmol g⁻¹ h⁻¹) and Ni-PNs (108.6 µmol g⁻¹ h⁻¹). Furthermore, 2D-2D heterojunction, CN-Pd(1:2) formed by coupling Pd-PNs with g-C₃N₄ exhibited a remarkably enhanced HER of 8400 μmol g⁻¹ h⁻¹, significantly higher than pristine Pd-PNs. This enhanced HER performance of heterojunction could be assigned to the synergistic interaction between Pd-PNs and g-C₃N₄, facilitating effective visible light absorption, facile charge separation, and migration with reduced recombination rates. The superior HER activity of CN-Pd(1:2) heterostructure was further established by transient photocurrent and timeresolved PL spectroscopy studies. This work highlights the importance of 2D-2D heterojunction photocatalysts for enhanced generation of green hydrogen by leveraging the cooperative effects between porphyrin MONs and g-C₃N₄.

Revisiting monetary policy transmission in a new inflation targeting country B Garg, SA Shah, J Edirisinghe - Journal of Asian Economics, 2025

53.

Abstract: We investigate the monetary policy transmission mechanism in Sri Lanka, which is gradually transitioning towards a flexible inflation targeting framework and has adopted this approach on a de facto basis. Using monthly data from 2020 to 2023, the findings highlight the interest rate channel as playing a more significant role than the exchange rate channel in transmitting the policy interventions to the final output. Key results suggest that under a strict inflation targeting regime, monetary transmission is more potent compared to a flexible inflation targeting framework. Therefore, to enhance monetary policy effectiveness, Sri Lanka should focus on the robust implementation of an inflation-targeting regime.

RMRDN: Recurrent multi-receptive residual dense network for image super-resolution **JS Sahambi** - Digital Signal Processing, 2025

Abstract: Reconstructing fine textures and structures from low-resolution images remains a central challenge in super-resolution (SR). Existing CNN-based SR models often suffer from limited receptive fields, weak long-range dependency modeling, and insufficient use of hierarchical features. To address these limitations, we propose a Recurrent Multi-Receptive Residual Dense Network (RMRDN) comprising three novel modules: (1) a Recurrent Multi-Receptive Residual Dense Block (RMRDB) for capturing rich contextual information; (2) a Residual Dense LSTM (RDLSTM) for long-range dependency modeling; and (3) a Relevant Feature Booster Block (RFBB) for effective hierarchical feature utilization. Extensive experiments on five benchmark datasets demonstrate that RMRDN outperforms existing methods by producing sharper textures and more accurate structural details. For ×4 upscaling, our proposed model outperforms the second-best SR method, achieving gains of +0.10 dB on Set5, +0.11 dB on Set14, +0.13 dB on BSD100, +0.06 dB on Urban100, and +0.11 dB on Manga109, respectively.

Some thermal properties of ideal gas

55.

56.

57.

RK Gupta, Meenu - The European Physical Journal C, 2025

Abstract: In this article, we investigate the thermal properties of non-relativistic many-body systems at finite temperatures and chemical potential. We compute the one-point function of various operators constructed out of the basic fields in ideal bosonic and fermionic many-body systems. The one-point function is non-zero only for operators with zero particle numbers. We investigate these operators in Rd and R+d, i.e. a flat space with a planar boundary. Furthermore, we compute the Green's function and using the operator product expansion, we express it in terms of the thermal one-point function of the higher spin currents. On R+d, the operator product expansion allows to express the bulk-bulk Green's function in terms of the thermal Green's function of the boundary operators. We also study the ideal system by placing it on curved spatial surfaces, specifically spherical surfaces. We compute the partition function and Green's function on spheres, squashed-sphere and hemispheres. Finally, we compute the large radius corrections to the partition function and Green's function by expanding in the large radius limit.

Sparse portfolio selection via topological data analysis based clustering A Goel, D Filipović, **P Pasricha** - Quantitative Finance, 2025

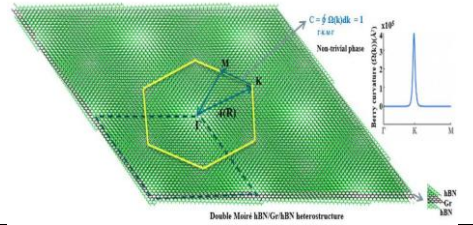
Abstract: This paper uses topological data analysis (TDA) tools and introduces a data-driven clustering-based stock selection strategy tailored for sparse portfolio construction. Our asset selection strategy exploits the topological features of stock price movements to select a subset of topologically similar (different) assets for a sparse index tracking (Markowitz) portfolio. We introduce new distance measures, which serve as an input to the clustering algorithm, on the space of persistence diagrams and landscapes that consider the time component of a time series. We conduct an empirical analysis on the S&P index from 2009 to 2022, including a study on the

COVID-19 data to validate the robustness of our methodology. Our strategy to integrate TDA with the clustering algorithm significantly enhanced the performance of sparse portfolios across various performance measures in diverse market scenarios.

Switching between topological phases in double moiré hBN-Graphene-hBN heterostructure with twist angles

Renu, K Katin, M Muruganathan, R Kumar - The Journal of Physical Chemistry C, 2025

Abstract: Twistronics in two-dimensional (2D) van der Waals heterostructures carries enormous potential for probing emergent quantum phases and tunable electronic behavior. In this study, we investigate the double moiré patterns for topological properties in a twisted hBN/Gr/hBN hybrid heterostructure using tight-binding approximations and DFT calculations. For smaller twist angles below $\Delta\theta < 5^{\circ}$, a reconstruction of the band structure is marked by formation of miniband gaps and multiple Dirac points from modification in the moiré wavelength and interference patterns. Closing and reopening of the band gaps are noted with twist angles. Further analyses of the Berry curvatures confirm a topological phase transition from a trivial (Chern number = 0) at $\Delta\theta = 0^{\circ}$ to a nontrivial phase (C = 1) at $\Delta\theta = 1.8^{\circ}$, and switching back to a trivial phase for $\Delta\theta > 5^{\circ}$. Our studies reveal twist angle driven topological phase transitions in 2D double moiré heterostructures, underscoring its applications in designing quantum devices.



<u>Terahertz label-free biomolecular sensing in quasi-bound states in a continuum metasurface</u> R KM, BK Bhowmik... **G Kumar -** Journal of the Optical Society of America B, 2025

Abstract: We present a terahertz metasurface that supports a quasi-bound state in the continuum (quasi-BIC) under symmetry-breaking effect, featuring sharp resonances ideal for biosensing applications. The design consists of an asymmetric bar pair structure supporting an antisymmetric dark mode that remains non-radiative (dark) under perfect mirror symmetry. Introducing in-plane mirror symmetry breaking with respect to the incident polarization transforms the dark mode into a quasi-BIC mode. The metasurface exhibits a sharp resonance on a flat transmission background, ensuring high spectral selectivity and contrast. The metasurface response was validated through simulations, coupled-mode theory, and terahertz time-domain spectroscopy. Biological analytes (human serum albumin, N-acetyl-L-tryptophanamide, and poly-L-lysine) were uniformly coated on the metasurface and experimentally analyzed for variation in the spectral shift. The results indicate a considerable resonance shift consistent with simulations. Unlike bare substrate measurements, which show negligible spectral change, the quasi-BIC resonance enables strong light-matter interaction and detection of minute refractive index variations. These results highlight the potential of quasi-BIC metasurfaces for highly sensitive, label-free biosensing in the terahertz regime.

59.

<u>Terahertz transmission anisotropy in e-textile</u> A Kumar, PK Sarswat ... **G Kumar**... - Optical Materials, 2025

60.

61.

Abstract: We present an experimental analysis of the intrinsic anisotropic terahertz transmission properties of a knitted industrial-grade electronic textile (e-textile) composed of polyethylene terephthalate and stainless-steel fiber-based yarns using terahertz time-domain spectroscopy. By changing the orientation of the e-textile with respect to the polarization and the angle of incidence of the terahertz radiation, we reveal a strong anisotropic behavior linked to the fabric's intrinsic axes defined by wale and course directions. The textile exhibits pronounced polarization and incident angle-dependent dichroism, alongside significant attenuation of the terahertz signal. Additional experiments on stacked textile layers further demonstrate the potential of e-textile for effective terahertz shielding. The complex refractive index confirms its dispersive and lossy nature, characteristic of hybrid metal-polymer composites. Furthermore, the observed anisotropic behavior is validated through simulations using effective medium theory and geometric modelling of the fabric's unit cell. We believe these results can contribute to a better understanding of the terahertz transmission characteristics of e-textiles and show their potential as flexible, passive materials for terahertz photonic and shielding applications, including in emerging 6G-related technologies.

<u>The microscopic mechanisms of high temperature oxidation of Haynes 282</u> G Ouyang, O Palasyuk, P Singh, **D Beniwal**... **PK Ray**... - Corrosion Science, 2025

Abstract: Nickel-based superalloy finds widespread applications in aerospace and extreme environments. They are known for their high temperature oxidation resistance under extended periods. However, the oxide formation and evolution which sets the stages for the later parabolic oxidation kinetics is not fully understood. This paper aims to provide new insights into the transient stage oxidation mechanism and kinetics of a typical Ni-based superalloy (Haynes 282). While tracking the chemical and microstructural evolution under micrometer scale at 800°C, we show that the oxide scale and its grain boundary species change significantly during the initial stages of oxidation and can have a profound impact on the oxidation kinetics. Cr₂O₃ forms initially at the grain boundary along with minor amount of Al₂O₃. Then, the grain boundary region is enriched with copious amounts TiO₂ while Cr migrates away from the grain boundary. A noticeable change in the isothermal oxidation kinetics observed likely results from a mechanistic change from uniform surface oxidation to preferential outward diffusion of Ti⁴ + ions through the grain boundary. Through first-principles calculations combined with energy dispersive spectroscopy, we confirmed the preferential outward diffusion of Ti⁴⁺ ions as the diffusion barrier is lower for Ti than Cr along the grain boundaries. These findings highlight the critical role of early-stage grain boundary oxidation dynamics in dictating the long-term oxidation resistance of Ni-based superalloys and provide a foundation for future strategies to enhance their performance in extreme environments.

<u>Transcendental nature of p-adic Euler-Lehmer constants</u> T Chatterjee, S Garg - Journal of Number Theory, 2025

Abstract: Murty and Saradha (2008) initiated a significant exploration into the transcendental nature of certain *p*-adic constants, focusing on the *p*-adic analogues of the Euler's constant and the Euler-Lehmer constant, where *p* is a rational prime with. Their work laid the foundation for understanding these constants in the context of *p*-adic analysis. This investigation was subsequently expanded by Chatterjee and Gun (2014), who extended the study to encompass the case of sets of prime numbers. In this article, we build upon their findings by generalizing the results further to include prime powers and products of prime powers. Our primary focus is to delve deeper into the transcendental properties of the *p*-adic analogues of the Euler-Lehmer constants in this broader framework.

63. Transwavenet: Transformer for underwater image restoration with wavelets

P Mishra, MDR Khan, SS Phutke, **SK Vipparthi**, S Murala - IEEE Transactions on Artificial Intelligence, 2025

Abstract: Underwater image restoration aims to improve the quality and visibility of images taken in underwater environments. These images find application in diverse fields like marine biology research, underwater archaeology, environmental monitoring, surveillance tasks, and offshore infrastructure inspection. However, the complexities of the underwater environment make these applications challenging, as light scattering and absorption cause blur, color cast, and reduced contrast in images. With the promising results on restoring underwater degraded images, existing approaches limit their performance in case of the above-mentioned complex and nonlinear degradation. In this research work, we propose a multi-directional wavelet coefficient space transformer model for underwater image deblurring and color restoration. Incorporating an attention mechanism within transformed spaces, our model dynamically adapts to underwater degradation. Additionally, we introduce a wavelet attention fusion transformer block for attention computation in the wavelet coefficient space, along with an edge-preserving wavelet downsampling block to retain fine details and textures during downsampling. A thorough assessment of our method on real-world (UCCS, U45, SQUID) and synthetic (UIEB, UCDD) datasets, along with profound ablation studies, validates its edge over existing techniques. Further, we have evaluated our method for tasks such as depth estimation, and low-light enhancement and deblurring, demonstrating its versatility and broad applicability across various image processing tasks. The code is made available at: https://github.com/Priyanka01mishra/TransWaveNet.

<u>Tunable broadband terahertz modulation in a multi-stacked toroidal metamaterial</u> BS Chouhan, S Ghosal...**G Kumar** - Physica Scripta, 2025

Abstract: Metamaterial-based photonic components are driving significant scientific and technological advancements in the terahertz (THz) frequency range. In this study, we present a multilayered metamaterial based on toroidal excitation for ultra-broadband THz modulation. The toroidal resonance within the stacked resonators enables subwavelength coupling with individual resonators, significantly broadening the transmission bandwidth. Our multi-stacked metamaterial demonstrates a full width at half maximum (FWHM) of 370 GHz, which is approximately 137% of the 270 GHz bandwidth of a single-layer metamaterial. A detailed multipolar analysis reveals that the toroidal dipole dominates the electromagnetic response, confirming the enhanced performance of the stacked configuration over its planar counterpart. Furthermore, by integrating a temperature-responsive vanadium dioxide (VO₂) layer into the multilayer structure, we enable tunable amplitude transmission through external thermal control. By varying the temperature of the VO₂ layer from 30 °C to 120 °C, we achieve a transition from a band-reject filter to a broadband reflector, as verified by experimentally obtained THz-TDS spectral results. In addition, we investigate the temporal switching dynamics of the modulator using time-resolved transmission measurements under periodic electrical pulsing. The device exhibits efficient and reversible electro-thermal modulation, with rise and fall times in the range of a few seconds, making it suitable for practical applications requiring dynamic THz control. This tunable and switchable THz modulator holds significant promise for broadband communication systems and adaptive photonic platforms.

<u>UAV-assisted IRS-aided network coded cooperation in 6 g wireless communication</u> P Kumar, N Goel, **S Darshi**, S Majhi... - IEEE Transactions on Vehicular Technology, 2025

64.

Abstract: In this paper, integration of intelligent reflecting surface (IRS) with unmanned aerial vehicle (UAV)-assisted network-coded cooperation (UA-NCC) system is proposed for improving the reliability of the infrastructure-less network in sixth generation (6 G) wireless communication. A mathematical framework is proposed by considering Nakagami-m fixed channel gain for ground-to-ground (G2G) links and height-dependent Nakagami-m channel gain for air-to-ground (A2G) links. Moreover, a cumulative distribution function (CDF) for end-to-end (E2E) signal-to-noise ratio (SNR) is derived for the proposed scheme, by considering the signal is reached the end users either through an IRS or via a UAV. Furthermore, an outage probability and its asymptotic behavior for the proposed system model are derived by considering the effect of both the signal coming via UAV as well as IRS elements in Nakagami-m fading environments. The findings demonstrate that the simulation results are aligned with our theoretical derivation, and it is also compared with the existing state-of-the-art.

<u>Understanding entrepreneurial thinking for designers: Perspectives from entrepreneurs, academicians, product designers, and students</u>

K Sandhu, P Sarkar, K Subburaj - Thinking Skills and Creativity, 2025

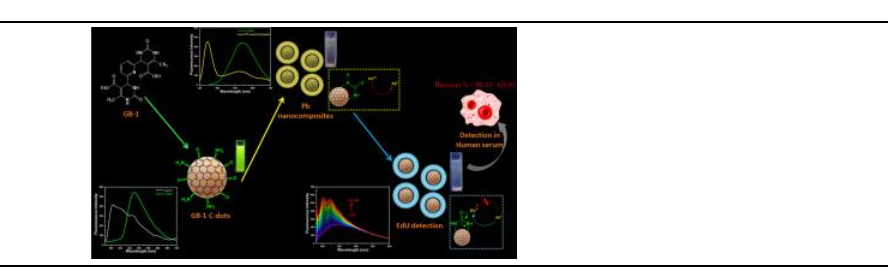
Abstract: Entrepreneurship education is increasingly vital across disciplines to equip students with the skills to address complex global challenges. However, a clear and unified understanding of entrepreneurial thinking, particularly within engineering education, remains lacking. This study aims to develop a comprehensive definition of entrepreneurial thinking suitable for integration into engineering curricula. We conducted semi-structured interviews with eleven participants, including entrepreneurs, academicians, and product designers from diverse fields, such as product design, textile, ergonomics, finance, biomedical engineering, computer science, and mechanical engineering. Using Natural Language Processing (NLP) techniques, specifically keyword extraction and topic modeling with Latent Semantic Indexing, we analyzed the interview transcripts to identify key terms and themes. From this analysis, we extracted the top 50 words and identified the top 20 topics related to entrepreneurial thinking. Brainstorming sessions with product designers were then held to construct definitions based on these findings. Through majority and relationship analysis, we derived a unified definition of entrepreneurial thinking. The final definition was compared with variations of definitions prepared by undergraduate design students, revealing that students had a vague understanding of the concept. To address this gap, we proposed a framework that integrates the developed definition with engineering course elements using the Lean Canvas Model. This framework aligns engineering education with entrepreneurial skills without adding a significant workload, serving as a practical tool for educators. This study provides a unified definition of entrepreneurial thinking and offers a practical framework for its integration into engineering education, thereby fostering an entrepreneurial mindset among future engineers.

<u>Unveiling EdU detection: Surfactant-free synthesis of Pb nanocomposites for spectroscopic probing in human serum</u>

G Bhardwaj, R Kaur, K Sharma, N Kaur, N Singh - Microchemical Journal, 2025

Abstract: Toxicity of lead ions has been increasing day by day in environment, plants and animals. Presence of lead in the river waters due to industrial waste has been increasing with increasing development. To tackle the problem, we have fabricated dihydropyrimidinedione (DHPMs) based C-dots which can detect Pb²⁺ ions with a detection limit of 2 nM which is less than the Environmental Protection System (EPS). The detection of Pb²⁺ has been done using UV–Visible spectrophotometer and fluorescence spectrometer. The complex formed between C-dots and Pb²⁺ was further reduced to yield core-shell nanocomposites, which were fully characterized using various analytical techniques. The formed Pb nanocomposites were stable and can be further used in the wide range of pH, salt and temperature. These Pb nanocomposites were used for the detection of cytotoxic ethynyldeoxyuridine in human serum with a detection limit of 4 nM, in the linear range of 1–160 nM with a standard deviation of ±5 and a recovery percentage of 102 %.

66.



Disclaimer: This publication digest may not contain all the papers published. Library has compiled the publication data as per the alerts received from Scopus and Google Scholar for the affiliation "Indian Institute of Technology Ropar" for the month of September, 2025. The author(s) are requested to share their missing paper(s) details if any, for the inclusion in the next publication digest.